JOURNAL OF AIRCRAFT
Vol. 40, No. 3, May–June 2003

Integrated Trim and Structural Design Process for Active Aeroelastic Wing Technology

P. Scott Zink,* Daniella E. Raveh,† and Dimitri N. Mavris‡
Georgia Institute of Technology, Atlanta, Georgia 30332-0150

A new method for concurrent trim and structural optimization of active aeroelastic wing technology is presented. The new process treats trim optimization and structural optimization as an integrated problem in which control surface gear ratios and structural design variables are posed together in the same optimization problem and act toward the same objective of weight minimization. This new design philosophy is in contrast to most existing active aeroelastic wing design processes in which structural optimization and trim optimization, each having their own different objectives and constraints, are performed in an iterative, sequential manner. The new integrated active aeroelastic wing design process is demonstrated on a lightweight fighter-type aircraft and compared to a more traditional, sequential active aeroelastic wing design process. For this demonstration, the integrated process converges to a lower weight and offers an advantage over the sequential process in that optimization is performed in one continuous run, whereas the sequential approach requires pausing and restarting the structural optimization to allow for trim optimization.

Nomenclature

[AICS]	=	aerodynamic influence coefficients matrix in structural degrees of freedom
$D_i\{\}$, $D_i[\,]$	=	partial derivative of a vector or matrix with respect to ith gear ratio, $\partial\{\}/\partial g_i$, $\partial[]/\partial g_i$
$\{F\}^{\text{aero}}$	=	vector of aerodynamic forces (including effects of flexibility) in discrete coordinates
$[G]$	=	gearing matrix
[GAIC]	=	generalized aerodynamic influence coefficients matrix
[GK]	=	generalized stiffness matrix
[GP]	=	rigid unit aerodynamics loads in generalized coordinates
g	=	gear ratio
$[I]$	=	identity matrix
$[K]$	=	stiffness matrix
L	=	lift
$[M]$	=	mass matrix
n_e	=	number of elastic modes
n_g	=	number of gear ratio design variables
n_m	=	number of sizing maneuvers
n_r	=	number of rigid-body modes
n_{st}	=	number of strain constraints per sizing maneuver
n_t	=	number of thickness design variables
$[P]$	=	matrix of rigid aerodynamic loads in discrete coordinates due to unit deflection of the aerodynamic trim parameters
q	=	dynamic pressure
t	=	structural thickness design variable
$\{u\}$	=	vector of structural displacements in discrete coordinates
$\{\ddot{u}_r\}$	=	vector of rigid-body accelerations in discrete coordinates
α	=	angle of attack
δ	=	control surface deflection
$\{\delta\}$	=	vector of aerodynamic trim parameter deflections, for example, angle of attack, control surface deflection, and roll rate
ε	=	strain
$\{\xi\}$	=	vector of modal displacements
$\{\ddot{\xi}\}$	=	vector of modal accelerations
$\{\phi\}$	=	mode of free vibration

Subscripts

allow	=	allowable
D	=	dependent trim parameter
e	=	elastic mode set
flex	=	includes effects of flexibility
HT	=	horizontal tail
I	=	independent trim parameter
LEI	=	leading-edge inboard control surface
LEO	=	leading-edge outboard control surface
r	=	rigid-body mode set
TEI	=	trailing-edge inboard control surface
TEO	=	trailing-edge outboard control surface

Superscripts

T	=	transpose
-1	=	inverse

Received 6 February 2001; revision received 18 June 2002; accepted for publication 20 June 2002.

*Ph.D. Candidate, School of Aerospace Engineering; currently Senior Aeronautical Engineer, Lockheed Martin Aeronautics Company, P.O. Box 748, Mail Zone 9382, Fort Worth, Texas 76101. Member AIAA.

†Research Engineer II, School of Aerospace Engineering; currently Senior Lecturer, Faculty of Aerospace Engineer, Technion–Israel Institute of Technology, Haifa, Israel 32000. Member AIAA.

‡Boeing Professor of Advanced Aerospace Systems Analysis, School of Aerospace Engineering. Associate Fellow AIAA.

Introduction

AN emerging and promising technology for addressing the problem of adverse aeroelastic deformation, such as control surface reversal, is active aeroelastic wing (AAW) technology. It has recently been a key area of study for both the government and industry[1,2] and is defined by Pendleton et al. as "a multidisciplinary, synergistic technology that integrates air vehicle aerodynamics, active controls, and structures together to maximize air vehicle performance."[3] AAW technology exploits the use of leading- and trailing-edge control surfaces to shape the wing aeroelastically, with the resulting aerodynamic forces from the flexible wing becoming the primary means for generating control power. With AAW,

the control surfaces then act mainly as tabs and not as the primary sources of control power as they do with a conventional control philosophy. As a result, wing flexibility is seen as an advantage rather than a detriment because the aircraft can be operated beyond reversal speeds and still generate the required control power for maneuvers. Hence, there is potential for significant reductions in structural weight and actuator power.

Figure 1 illustrates conceptually the differences between AAW technology and a conventional control approach for a rolling maneuver. The hypothetical example shows the cross section of two wings deforming due to aeroelastic effects. The upper wing, employing AAW technology, is twisting in a positive way with the use of both leading- and trailing-edge surfaces, whereas the conventionally controlled, lower wing, which uses only the trailing-edge surface, is twisting in a negative way.[4] This adverse twist due to the deflection of the trailing-edge surface is associated with reduced control surface effectiveness and control surface reversal, in which the increase in camber due to the deflection of the surface is offset by the negative twist of the wing.[5]

In consideration of AAW technology's use of redundant control surfaces, an important constituent of the technology are control surface gear ratios that dictate how one control surface deflects with respect to a single basis surface. Two gear ratio scenarios are illustrated in Fig. 2 in which the deflections of the leading-edge inboard (LEI), leading-edge outboard (LEO), and trailing-edge inboard (TEI) surfaces are linearly dependent on the deflection of the trailing-edge outboard surface (TEO). The gear ratios, which determine these dependencies, are circled in Fig. 2. This concept is also referred to as control surface blending and, for the purposes of this research, constitute the control laws.

With the use of AAW technology, it is desirable to design the gear ratios for a given maneuver to redistribute the aeroelastic loads favorably while meeting maneuver demands within actuator and control surface limits. Because the gear ratios influence the aeroelastic load distribution, the optimal structural design will be heavily dependent on the gear ratios selected. In turn, the optimal gear ratio values are dependent on the structural design. As a result, there is a heavy interdependency between the design of the gear ratios and structure. This multidisciplinary problem forms the heart of the AAW design process, which is defined here as concurrent structural and trim optimization. Structural optimization refers to the sizing of structural elements, for example, skin thickness and spar thickness, to minimum weight, subject to stress, aeroelastic constraints, etc. Trim optimization refers to the process of selecting the gear ratios, or control surface deflection angles, that trim the aircraft to a prescribed maneuver while optimizing a certain objective function within actuator limits. The need for trim optimization is due to AAW technology's use of redundant control surfaces, which means that the static aeroelastic trim equations cannot be solved in a closed-form manner. Much research has been done in the area of trim optimization, where Refs. 6–10 discuss several approaches by which this problem has been addressed.

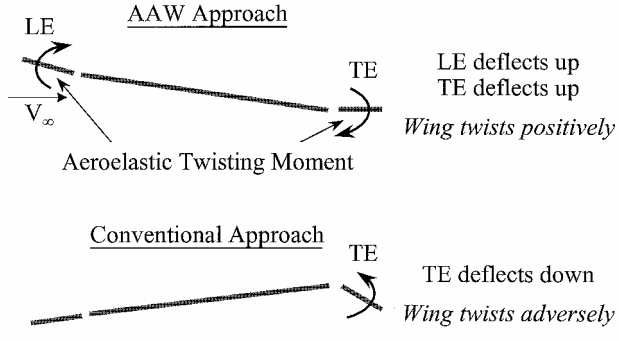

Fig. 1 AAW technology vs conventional control.

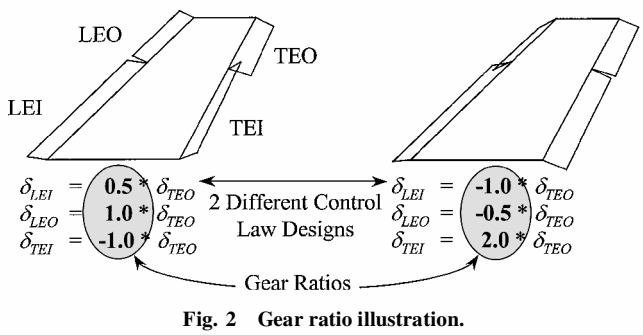

Fig. 2 Gear ratio illustration.

The literature dealing with the AAW design process is more limited. Most of the methods that have been developed are those in which trim optimization and structural optimization are separate optimization problems, each with their own unique objectives, constraints, and design variables, performed in a sequential, iterative manner. For the purposes of this paper, this type of AAW design process is referred to as a sequential AAW design process. Zillmer[11] and Dobbs et al.[12] developed such an approach. In this case, trim optimization, performed using the Integrated Structure/Maneuver Design (ISMD) program, is embedded in an iterative process with NASTRAN.[13] The control surface deflections, in ISMD, are optimized to minimize a composite function of stress, induced drag, and buckling load. The maneuver loads resulting from the optimized control surface deflections of ISMD are transferred to NASTRAN, which then optimizes the structure to minimum weight. NASTRAN then passes stability derivatives and sensitivity information of the current structural design to ISMD for another trim optimization. This process repeats itself until the wing weight converges.

Another example, in the literature, of a sequential AAW design process is found in Ref. 9. In this case, the trim optimization module, in which the deflection of the control surfaces are optimized to minimize user-defined component loads (e.g., root bending moment and hinge moment), is placed within the structural optimization loop of ASTROS,[14] a finite element-based structural optimization code. For each iteration in the structural optimization, the control surface deflections for the current structural design are optimized. Then, with these new deflections, the structural optimizer proceeds to take another step, pauses again for trim optimization, and so on, until the structural optimization objective, wing weight, converges.

Zink et al.[15] applied the techniques of Ref. 9 in a design study of a generic lightweight fighter concept employing AAW technology, with four wing control surfaces and a horizontal tail. Trim optimization was performed for antisymmetric (rolling) and symmetric maneuvers. The trim optimization problem for the symmetric maneuver was posed as a minimization of root bending moment (RBM), whereas a summation of the wing hinge moments was the objective for the antisymmetric maneuvers. It was solved using a gradient-based optimization algorithm. The intention was that trim and structural optimization would be repeated iteratively. However, only the first step was demonstrated because trim optimization was performed only once on the starting structural design. As an evolution of the work in Ref. 15, a new sequential AAW design process was developed that employs the simplex method[16] for trim optimization. This new sequential process is reviewed briefly in the current work and documented in detail in Ref. 10.

Miller[6] proposed an AAW design process in which the thickness of the structural elements and the control surface deflections were simultaneous design variables in an integrated optimization problem. The objective of this approach was the minimization of weight, subject to trim balance requirements, stress constraints, and buckling load constraints. This approach represents a diversion from the previous AAW design processes because, in this case, trim optimization and structural optimization were not separate problems.

In the current research, a similar AAW design process is developed in which trim and structural optimization are treated together as an integrated optimization problem acting toward the same objective. However, in this approach, the control surface gear ratios, rather than their deflections, are included alongside structural design variables in the optimization problem whose objective is weight minimization. Additionally, hinge moments are included in the optimization problem as constraints. The possible advantages of the

integrated AAW design process include better solution convergence and lower weight structural designs. Its development and comparison with the sequential AAW design process of Ref. 10 on a generic lightweight fighter is the goal of the current effort.

Methodology

Integrated AAW Design Process

The integrated AAW design process is formulated formally as the following optimization problem:

Minimize weight subject to material strain allowables,

$$\varepsilon_{ji} \le \varepsilon_{\text{allow}}, \qquad j = 1, \ldots, n_{\text{st}}, \qquad i = 1, \ldots, n_m \tag{1}$$

control surface travel limits,

$$\begin{aligned} -30 \le \delta_{\text{LEI}_j} \le 5 \text{ deg}, \qquad & -30 \le \delta_{\text{LEO}_j} \le 5 \text{ deg} \\ -30 \le \delta_{\text{TEI}_j} \le 30 \text{ deg}, \qquad & -30 \le \delta_{\text{TEO}_j} \le 30 \text{ deg} \\ -30 \le \delta_{\text{HT}_j} \le 30, \qquad & j = 1, \ldots, n_m \end{aligned} \tag{2}$$

and hinge moment constraints,

$$\begin{gathered} -3.0 \times 10^5 \le \text{HM}_{\text{LEI}_j} \le 3.0 \times 10^5 \\ -1.0 \times 10^5 \le \text{HM}_{\text{LEO}_j} \le 1.0 \times 10^5 \\ -1.5 \times 10^5 \le \text{HM}_{\text{TEI}_j} \le 1.5 \times 10^5 \\ -5.0 \times 10^4 \le \text{HM}_{\text{TEO}_j} \le 5.0 \times 10^4, \qquad j = 1, \ldots, n_m \end{gathered} \tag{3}$$

in inch pounds, with the design variables

$$t_i: \quad i = 1, \ldots, n_t, \qquad g_j: \quad j = 1, \ldots, n_g$$

The preceding optimization problem is implemented in modal-based ASTROS, which provides efficient and accurate finite element-based static aeroelastic analysis and optimization.[17,18] The optimization is based on the hybrid modal approach in which trim is computed in modal coordinates, whereas stress analysis is performed in discrete coordinates for greater accuracy. The optimization problem is solved by the modified method of feasible directions[19] algorithm. At the heart of the modal approach is the representation of the discrete displacements as a linear combination of the free aircraft low-frequency modes of vibration, which are then used to create the generalized stiffness, mass, and force matrices that comprise the static aeroelastic equation. Modal-based static aeroelastic equations are assembled for each maneuver to which the structure and gear ratios are designed and are then solved to evaluate the preceding constraints. In addition, the static aeroelastic equation is used to derive analytical sensitivities of the constraints with respect to the design variables, as opposed to numerical sensitivities calculated through finite differencing. These sensitivities are used in the optimization algorithm. Use of the modal approach, along with analytic sensitivities, then reduces the size of the analysis and optimization problem significantly.

Although the structural weight is not an explicit function of the gear ratios, the stress/strain, hinge moment, and control surface deflection constraints are. It is, thus, through the constraints that the gear ratios can be used to lower the weight over the course of the optimization. As a result, the sensitivities of these constraints with respect to each of the gear ratios of interest for each maneuver are required. Analytical sensitivities of these constraints have been derived for the static aeroelastic equation in modal coordinates, and their derivations are provided in the following sections. The derivation of the sensitivities of the objective and constraints with respect to the thickness variables, in addition to solution of the modal-based static aeroelastic equation for constraint evaluation, is provided in Ref. 20 and will not be repeated here.

Gear Ratio Sensitivities

The basic equation for the static (or quasi-steady) aeroelastic analysis of a maneuvering aircraft by the finite element method in discrete coordinates is[21]

$$[[K] - q[\text{AICS}]]\{u\} + [M]\{\ddot{u}_r\} = [P]\{\delta\} \tag{4}$$

Equation (4) is transformed to modal coordinates by assuming that the displacements $\{u\}$ are a linear combination of the low-frequency modes of vibration, as given by

$$\{u\} = [\phi_r \quad \phi_e] \begin{Bmatrix} \xi_r \\ \xi_e \end{Bmatrix} \tag{5}$$

where $[\phi_r \ \ \phi_e]$ is the modal matrix comprising the rigid-body modes $[\phi_r]$ and a subset of the elastic modes $[\phi_e]$. Substitution of Eq. (5) into Eq. (4) and premultiplication of Eq. (4) by the transpose of the modal matrix yields the static aeroelastic equation in modal coordinates[20]:

$$\begin{bmatrix} -q\,\text{GAIC}_{\text{rr}} & & -q\,\text{GAIC}_{\text{re}} \\ -q\,\text{GAIC}_{\text{er}} & \text{GK}_{\text{ee}} & -q\,\text{GAIC}_{\text{ee}} \end{bmatrix} \begin{Bmatrix} \xi_r \\ \xi_e \end{Bmatrix} + \begin{bmatrix} M_{\text{rr}} \\ M_{\text{er}} \end{bmatrix} \{\ddot{\xi}_r\} = \begin{bmatrix} \text{GP}_r \\ \text{GP}_e \end{bmatrix} \{\delta\} \tag{6}$$

When it is considered that with AAW technology $\{\delta\}$ contains a redundant number of aerodynamic trim parameters, a gearing matrix is introduced to define the following relationship:

$$\{\delta\} = \begin{Bmatrix} \delta_D \\ \delta_I \end{Bmatrix} = \begin{bmatrix} G \\ I \end{bmatrix} \{\delta_I\} = [G]^*\{\delta_I\} \tag{7}$$

The matrix $[G]$ contains the gear ratios g_i and relates the redundant (dependent) trim parameters $\{\delta_D\}$ to the determinate (independent) ones $\{\delta_I\}$. The number of independent trim parameters must equal the number of rigid-body degrees of freedom (DOF). In general, $[G]$ can be a full matrix, meaning that the dependent control surfaces can be dependent on more than one independent trim parameter. However, in this study, the dependent surfaces are geared to only one independent control surface.

Equation (7) is substituted into the right-hand side of Eq. (6). Then, taking the derivative of Eq. (6) (where $[\text{GPG}] = [\text{GP}][G]^*$) with respect to the ith gear ratio and combining left-hand terms results in the following:

$$\begin{bmatrix} -q\,\text{GAIC}_{\text{rr}} & & -q\,\text{GAIC}_{\text{re}} & M_{\text{rr}} \\ -q\,\text{GAIC}_{\text{er}} & \text{GK}_{\text{ee}} & -q\,\text{GAIC}_{\text{ee}} & M_{\text{er}} \end{bmatrix} \begin{Bmatrix} D_i\{\xi_r\} \\ D_i\{\xi_e\} \\ D_i\{\ddot{\xi}_r\} \end{Bmatrix} = \begin{bmatrix} \text{GPG}_r \\ \text{GPG}_e \end{bmatrix} D_i\{\delta_I\} + \begin{bmatrix} D_i[\text{GPG}_r] \\ D_i[\text{GPG}_e] \end{bmatrix} \{\delta_I\} \tag{8}$$

Equation (8) is a system of $n_r + n_e$ equations with $2n_r + n_e$ unknown sensitivities. Here $\{\delta_I\}$ is known because we are differentiating about a known static aeroelastic equilibrium condition, and the sensitivity terms, $D_i[\text{GPG}_r]$ and $D_i[\text{GPG}_e]$, are known as well. This is because they are the columns of $[\text{GP}_r]$ and $[\text{GP}_e]$, respectively, that correspond to the ith gear ratio. For example, if the rigid-body accelerations $\{\ddot{\xi}_r\}$ are defined by the user for a specific maneuver, then $D_i\{\ddot{\xi}_r\}$ is zero because the accelerations are constant. In this case, then, the unknown sensitivities are the n_e elements of $D_i\{\xi_e\}$, the n_r elements of $D_i\{\xi_r\}$, and the n_r elements of $D_i\{\delta_I\}$, which are more unknowns than equations available to solve them. These unknown sensitivities are solved using an unrestrained formulation in which an additional equation is introduced that is based on the assumption that the displacement $\{u\}$ does not change the location of the center of gravity or orientation of the mean axis system, which defines the alignment of the aircraft moments of inertia.[22] As presented by Rodden and Love,[22] this assumption yields an equation

in which the rigid-body modes $[\phi_r]$ are orthogonal to the displacement vector $\{u\}$ with respect to the mass matrix. Expressed in modal coordinates, this leads to the following equation:

$$[M_{rr}]\{\xi_r\} + [M_{er}]^T\{\xi_e\} = \{0\} \tag{9}$$

Differentiating with respect to g_i, Eq. (9) becomes

$$[M_{rr}]D_i\{\xi_r\} + [M_{er}]^T D_i\{\xi_e\} = \{0\} \tag{10}$$

Solving for $D_i\{\xi_r\}$

$$D_i\{\xi_r\} = -[M_{rr}]^{-1}[M_{er}]^T D_i\{\xi_e\} \tag{11}$$

When Eq. (11) is substituted into Eq. (8), Eq. (8) becomes

$$\begin{bmatrix} q[\mathrm{GAIC}_{rr}][M_{rr}]^{-1}[M_{er}]^T - q[\mathrm{GAIC}_{re}] & [M_{rr}] \\ q[\mathrm{GAIC}_{er}][M_{rr}]^{-1}[M_{er}]^T + [\mathrm{GK}_{ee}] - q[\mathrm{GAIC}_{ee}] & [M_{er}] \end{bmatrix}$$

$$\times \begin{Bmatrix} D_i\{\xi_e\} \\ D_i\{\ddot{\xi}_r\} \end{Bmatrix} = \begin{bmatrix} \mathrm{GPG}_r \\ \mathrm{GPG}_e \end{bmatrix} D_i\{\delta_I\} + \begin{bmatrix} D_i[\mathrm{GPG}_r] \\ D_i[\mathrm{GPG}_e] \end{bmatrix}\{\delta_I\} \tag{12}$$

Equation (12) now reflects a set of $n_r + n_e$ equations with $n_r + n_e$ unknowns, which are the elements of $D_i\{\delta_I\}$ and $D_i\{\xi_e\}$. Taking the second row of Eq. (12) and solving for $D_i\{\xi_e\}$ results in

$$D_i\{\xi_e\} = [\mathrm{GKA}_{ee}]^{-1}([\mathrm{GPG}_e]D_i\{\delta_I\} - [M_{er}]D_i\{\ddot{\xi}_r\} + D_i[\mathrm{GPG}_e]\{\delta_I\}) \tag{13}$$

where

$$[\mathrm{GKA}_{ee}] = q[\mathrm{GAIC}_{er}][M_{rr}]^{-1}[M_{er}]^T + [\mathrm{GK}_{ee}] - q[\mathrm{GAIC}_{ee}] \tag{14}$$

When Eq. (13) is substituted into the first row of Eq. (12), and the terms are rearranged the first row of Eq. (12) can be written as

$$[L]D_i\{\ddot{\xi}_r\} = [R]D_i\{\delta_I\} + D_i[R]\{\delta_I\} \tag{15}$$

where

$$[L] = [M_{rr}] + q[\mathrm{GAIB}_{re}][\mathrm{GKA}_{ee}]^{-1}[M_{er}] \tag{16}$$

$$[R] = [\mathrm{GPG}_r] + q[\mathrm{GAIB}_{re}][\mathrm{GKA}_{ee}]^{-1}[\mathrm{GPG}_e] \tag{17}$$

$$D_i[R] = D_i[\mathrm{GPG}_r] + q[\mathrm{GAIB}_{re}][\mathrm{GKA}_{ee}]^{-1}D_i[\mathrm{GPG}_e] \tag{18}$$

$$[\mathrm{GAIB}_{re}] = [\mathrm{GAIC}_{re}] - [\mathrm{GAIC}_{rr}][M_{rr}]^{-1}[M_{er}]^T \tag{19}$$

Equation (15) is used to solve for the n_r unknown trim sensitivities $D_i\{\delta_I\}$. These sensitivities are calculated through algebraic manipulation of Eq. (15) and are substituted into Eq. (13) to find the elastic modal displacement sensitivities $D_i\{\xi_e\}$. The rigid modal displacement sensitivities $D_i\{\xi_r\}$ are then estimated by substitution of $D_i\{\xi_e\}$ into Eq. (11). Once the sensitivities for the modal displacements are found, the sensitivities for stress and strain can be easily calculated by multiplying the modal displacement sensitivities by the fixed strain-displacement, stress-displacement transformation matrices.

Sensitivity of Dependent Surface Deflections

The control surface deflection constraints required significant modification to the ASTROS solution sequence. In the unmodified version of ASTROS, the independent control surface deflections could be directly constrained, and, because the gear ratios remained fixed in a conventional structural optimization, the dependent surface deflections could be constrained as well, through the constraint on the independent surface. However, with the integrated AAW design process, in which the gear ratios change with every iteration, the dependent surfaces could not be directly constrained. As a result, a new capability was added so that the dependent surface deflections could be directly constrained. This required the addition of a new constraint type and sensitivity calculation of the dependent surface deflection with respect to the gear ratios and structural design variables.

The deflection of a dependent control surface δ_{Dj} is given by the following equation:

$$\delta_{Dj} = g_j \cdot \delta_I \tag{20}$$

where g_j is its corresponding gear ratio and δ_I is the independent surface to which it is geared, whose deflection is found through solution of the static aeroelastic equation of motion [Eq. (6)]. The sensitivity, then, of the dependent surface deflection with respect to an arbitrary gear ratio design variable g_i is calculated by

$$\frac{\partial \delta_{Dj}}{\partial g_i} = \begin{cases} g_j \cdot \dfrac{\partial \delta_I}{\partial g_i} & i \neq j \\ \delta_I + g_j \cdot \dfrac{\partial \delta_I}{\partial g_i} & i = j \end{cases} \tag{21}$$

where $\partial\delta_I/\partial g_i$ is found from $D_i\{\delta_I\}$ in Eq. (15), and the second line of Eq. (21) corresponds to the sensitivity of the dependent surface deflection with respect to its own gear ratio.

The sensitivity of the dependent surface deflection with respect to a structural design variable t_i is given by

$$\frac{\partial \delta_{Dj}}{\partial t_i} = g_j \cdot \frac{\partial \delta_I}{\partial t_i} \tag{22}$$

Sensitivity of Aerodynamic Loads

The total aerodynamic loads (including the effect of flexibility) on the structural grid are[20]

$$\{F\}^{\mathrm{aero}} = q[\mathrm{AICS}][\phi_r \quad \phi_e]\begin{Bmatrix} \xi_r \\ \xi_e \end{Bmatrix} + [P][G]^*\{\delta_I\} \tag{23}$$

When Eq. (23) is differentiated with respect to g_i, Eq. (23) becomes

$$D_i\{F\}^{\mathrm{aero}} = q[\mathrm{AICS}][\phi_r \quad \phi_e]\begin{Bmatrix} D_i\{\xi_r\} \\ D_i\{\xi_e\} \end{Bmatrix} + [P][G]^* D_i\{\delta_I\} + D_i([P][G]^*)\{\delta_I\} \tag{24}$$

The sensitivities of the hinge moment constraints can then be found by multiplying $D_i\{F\}^{\mathrm{aero}}$ by an appropriate transformation matrix that represents the moment arm and that remains fixed throughout the optimization. These sensitivities are also required for discrete stress analysis in the hybrid modal approach.[20] The analytical sensitivities presented here have been verified by comparing them with sensitivities estimated by numerical differentiation (using finite differences).

Sequential AAW Design Process

The sequential AAW design process of Ref. 10 is performed by iterating between trim optimization, by the simplex method in MATLAB®[23] and structural optimization by modal-based ASTROS, as presented in Fig. 3. For each structural optimization iteration, the control surface deflections for the current structural design are optimized (represented by the MATLAB block). Then, these new control surface deflections are converted to gear ratios and passed to ASTROS, which reassembles the static aeroelastic equations with the new gear ratios. ASTROS then performs structural redesign to reduce weight using the optimization algorithm of Ref. 19. After the structural optimization step, the aeroelastic equations for the new structural design are assembled, and the appropriate stability derivatives, trim objective, and constraint sensitivities are calculated in ASTROS and then output to trim optimization. This process repeats itself until the structural optimization objective, wing weight, is converged.

Trim optimization, for the symmetric maneuvers of Ref. 10, is posed as a minimization of RBM, where the wing control surfaces are used to tailor the load distribution and provide load relief at the wing root, thus ultimately reducing wing weight. For the antisymmetric maneuvers, the objective of trim optimization is to minimize

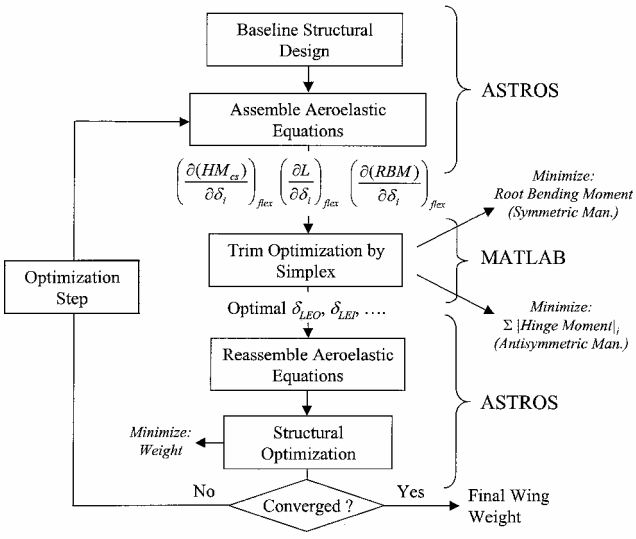

Fig. 3 Sequential AAW design process.[10]

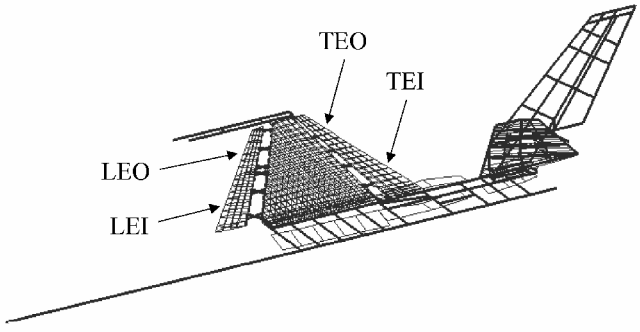

Fig. 4 Structural model of generic fighter.

a summation of the absolute value of each control surface hinge moment, as given by minimizing

$$|\mathrm{HM_{LEI}}| + |\mathrm{HM_{LEO}}| + |\mathrm{HM_{TEI}}| + |\mathrm{HM_{TEO}}| \tag{25}$$

This objective can be converted to linear programming form[24] by a simple transformation of the optimization problem. The details of this are reported in Ref. 10.

Numerical Example

Structural and Aerodynamic Model

The structural model of the aircraft used both in this research and in Ref. 10 is shown in Fig. 4. It is an ASTROS preliminary design finite element model of a lightweight composite fighter aircraft with four wing control surfaces (two trailing edge and two leading edge) and a horizontal tail.[17,25] It corresponds to a wing with an aspect ratio of 3.0, a total planform area of 330 ft^2, a taper ratio of 20%, a leading-edge sweep of 38.7 deg, and a thickness ratio of 3%. The skin of the wing is made up of a symmetric composite laminate, with only membrane stiffness, that comprises 0-, ± 45-, and 90-deg plies. The thickness of the −45- and +45-deg plies are constrained to be equal. The number of discrete DOF is approximately 3700, whereas the number of modes that serve as generalized coordinates for both symmetric and antisymmetric boundary conditions is 35. This relatively high number of modes is due to the use of the modal approach for strength analysis, which typically requires more modes than dynamic analysis.

The aerodynamic model is shown in Fig. 5. It is a flat-panel Carmichael[26] model containing 143 vertical panels and 255 horizontal panels. It also contains paneling for the four wing control surfaces and horizontal tail to coincide with the control surfaces on the structural model. Carmichael aerodynamic influence coefficients

Table 1 Maneuver conditions and design constraints

Maneuver condition	Design constraint
1) Mach 0.95, 10,000 ft, 9-g pullup	Fiber strain: 3000 $\mu\varepsilon$ tension 2800 $\mu\varepsilon$ compression
2) Mach 1.20, sea level, -3-g pushover	Fiber strain: 3000 $\mu\varepsilon$ tension 2800 $\mu\varepsilon$ compression
3) Mach 1.20, sea level, steady-state roll at 100 deg/s	Fiber strain: 1000 $\mu\varepsilon$ tension 900 $\mu\varepsilon$ compression
4) Mach 0.95, 10,000 ft, steady-state roll at 180 deg/s	Fiber strain: 1000 $\mu\varepsilon$ tension 900 $\mu\varepsilon$ compression

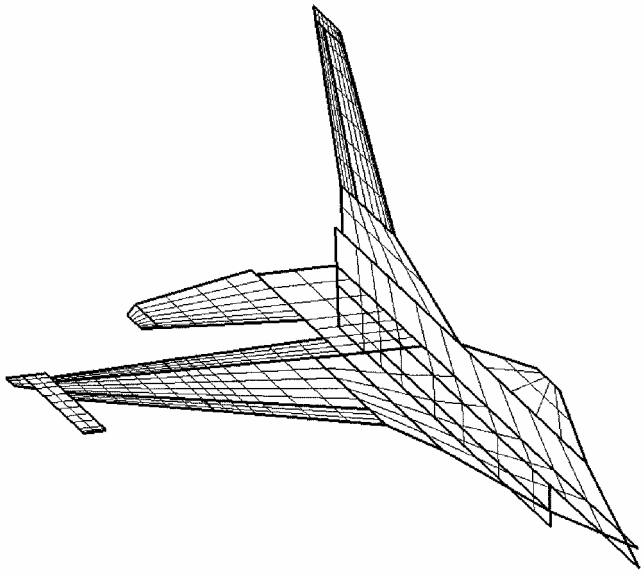

Fig. 5 Aerodynamic model of generic fighter.

are produced for two Mach numbers, 0.95 and 1.2, for both symmetric and antisymmetric maneuvers (see Ref. 27).

The structural design variables t_i in the AAW design process are the layer thickness of the wing box composite skins. The number of structural design variables is 78 due to physical linking of the skin elements. Internal structure and carry-through structure remain fixed. Table 1 shows the maneuver conditions and strength constraints to which the structure is designed for both the sequential and integrated AAW design processes. The maneuvers considered are two-DOF symmetric (i.e., balance of lift and pitching moment) and one-DOF antisymmetric (i.e., balance of rolling moment) steady-state maneuvers. The strength constraints are applied only to the skin elements that are designed, where the strain in each of the four plies is a separate constraint. This results in 3808 strain constraints per maneuver. Although a realistic fighter design requires the consideration of asymmetric three-DOF rolling pullout maneuvers, this study is limited to pure symmetric and antisymmetric maneuvers for simplicity. To account for this, the strength constraints of the antisymmetric maneuvers are lowered, acknowledging that additional strain will result from the symmetric component of the asymmetric maneuver. In addition to the strength constraints, hinge moment constraints and control surface travel limits are also included, as given earlier in Eqs. (2) and (3). These hinge moment and travel limits are based on typical allowables for modern fighter aircraft.

The gear ratio design variables of the integrated process, for each maneuver, are shown in Table 2, along with the independent surface for each maneuver to which the dependent surfaces are geared. For example, the variable g_{LEI3} is the ratio of the deflection of the LEI surface to the deflection of the LEO surface for the supersonic roll. The horizontal tail is selected as the independent surface for maneuvers 1 and 2 because it has historically been the primary

control surface for symmetric trim. The LEO surface is selected for maneuver 3 because it is the most effective surface at supersonic conditions, at which point both trailing-edge surfaces experience control reversal. For maneuver 4, the TEO surface is the independent surface because it is the most effective roll control surface at subsonic speeds.

Results

The integrated AAW design process, as proposed herein, has been implemented in modal-based ASTROS and demonstrated on the model discussed earlier. It is compared with the sequential AAW design process, discussed in detail in Ref. 10. As shown in Table 3, a comparison of the optimal weights by each approach reveals that the integrated approach converges to a significantly lower (15% less) weight. The weight presented here corresponds only to those structural elements that were designed, namely, the wing box skins. The integrated approach converges to its solution in 10 iterations, whereas the sequential approach takes six iterations.

Figure 6 shows a comparison of the optimal total upper surface skin thickness of the wing box by the integrated and sequential AAW design processes. The thickness displayed is a summation of the optimal thickness of all four composite plies, and the shaded regions show those zones of the wing box skins that were linked together as single design variables for the purposes of reducing the size of the design task. A cursory examination of Figs. 6a and 6b reveals, as expected, that thinner skins result from the integrated approach. In particular, one observes rather dramatic reductions in skin thickness in the middle and outboard sections of the wing. However, at the wing roots, the two approaches result in comparable skin thickness. This is most likely attributed to the sequential approach's minimization of RBM for the subsonic pullup maneuver, which is the maneuver that typically sizes the inboard part of the wing. Minimization of the bending moment at the wing root dramatically relieves internal load in this region, but it does not necessarily relieve load as much in other parts of the wing. Hence, one observes that the sequential approach with the minimization of RBM as the trim optimization objective results in comparable skin thickness at the wing root, but fails to compete with the integrated approach in other parts of the wing. This leads to a beneficial property of the integrated approach, which is that it provides weight savings to all parts of the wing by acting at the element level to relieve strain, whereas with the sequential approach, dependent on the choice of the trim optimization objective, weight savings tend to be more concentrated in local areas. Similar trends in the optimal skin thickness between the integrated and sequential AAW design process are found on the lower surface, as well, which for length considerations are not presented here, though they can be found in Ref. 28.

Figure 7 shows the iteration history of the gear ratio design variables by both the sequential and integrated AAW design processes for the subsonic pullup. Table 4 shows the final control surface deflections, which are simply the trimmed values of the independent surface (in this case the horizontal tail) multiplied by the corresponding gear ratios. Experience shows that the best starting values for the gear ratio design variables are those as found by trim optimization of the sequential approach for the baseline, that is, starting, structural design. An exception to this guideline is found in the TEI surface of Fig. 7, in which the best starting value for g_{TEI1} was $+10.0$ (instead of -2.26 as in the sequential approach).

The two approaches, based on examination of Fig. 7, produce quite different gearing scenarios, though they both deflect the outboard surfaces (LEO and TEO) to their maximal negative values (nose down for the leading edge, tail up for the trailing edge). This has a tendency to shift the center of pressure inboard, thus relieving RBM (for the sequential approach) as well as strain (for the integrated approach) at the wing root. However, the two approaches differ in their use of the TEI surface, with the sequential approach

Table 2 Gear ratio design variables

Maneuver	Independent surface	Gear ratio design variables
1	HT	g_{LEI1}, g_{LEO1}, g_{TEI1}, g_{TEO1}
2	HT	g_{LEI2}, g_{LEO2}, g_{TEI2}, g_{TEO2}
3	LEO	g_{LEI3}, g_{TEI3}, g_{TEO3}
4	TEO	g_{LEI4}, g_{LEO4}, g_{TEI4}

Table 3 Final weights for each AAW design process

AAW design process	Weight, lb
Sequential	292.3
Integrated	248.0

Table 4 Final control surface deflections for subsonic pullup

Trim parameter	Sequential, deg	Integrated, deg
δ_{LEI1}	−4.61	−11.52
δ_{LEO1}	−30.06	−30.00
δ_{TEI1}	−6.45	29.86
δ_{TEO1}	−30.06	−30.00
δ_{HT1}	0.79	2.05
α_1	11.75	9.31

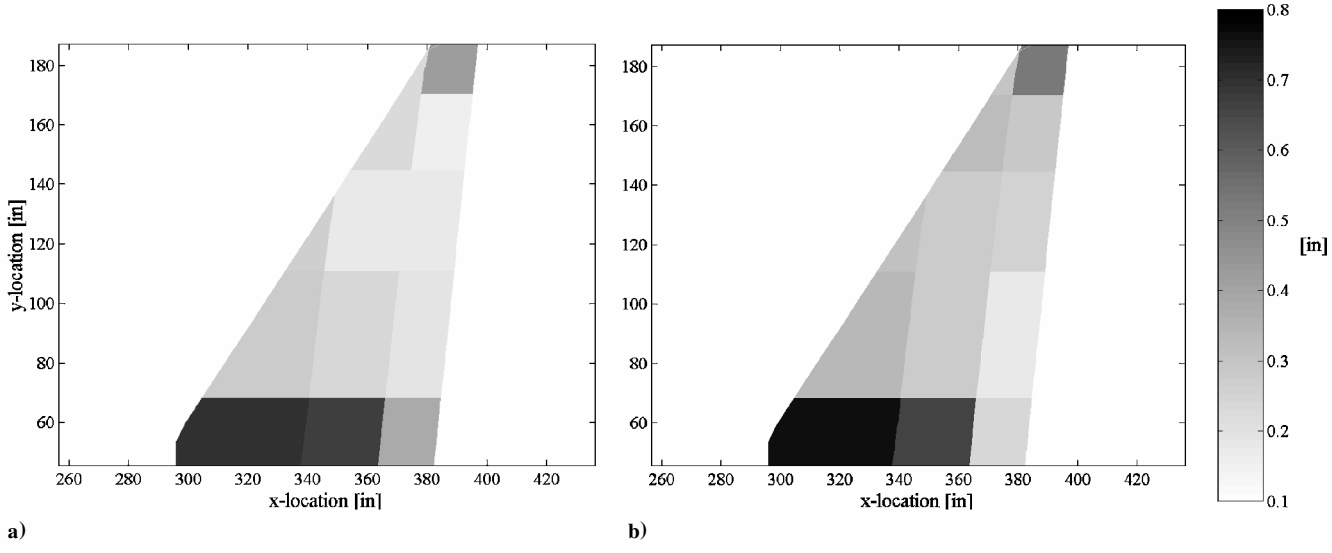

Fig. 6 Comparison of optimal total upper skin thickness by a) integrated approach and b) sequential approach.

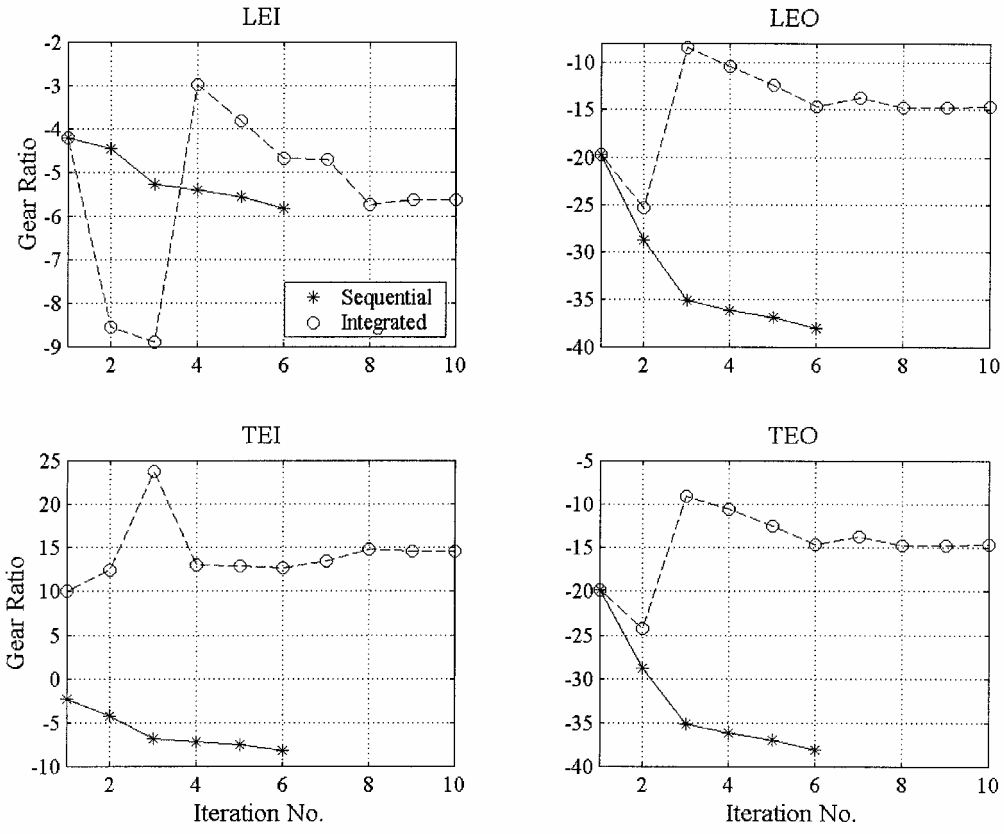

Fig. 7 Gear ratio history, subsonic pullup.

Table 5 Final gear ratios for supersonic roll

Gear ratio	Sequential	Integrated
g_{LEI3}	0.15	0.69
g_{TEI3}	0.007	0.022
g_{TEO3}	0.23	0.58

Table 6 Final control surface deflections for subsonic roll

Trim parameter	Sequential, deg	Integrated, deg
δ_{LEI4}	3.17	5.00
δ_{LEO4}	5.02	5.00
δ_{TEI4}	−2.39	19.06
δ_{TEO4}	15.29	6.75

using it in a negative fashion to reduce local lift forces. The integrated approach, which operates at a lower angle of attack for less loading throughout the wing, deflects the TEI all of the way down (positively) to get more lift from the control surface.

Another interesting feature of the gearing scenario for this maneuver is that both the sequential and integrated approach deflect the horizontal tail positively. This stands in stark contrast to a conventional approach in which the horizontal tail (which is typically the only surface used for symmetric trim) is deflected in a negative manner to provide pitchup moment to counteract the negative pitching moment produced by lift on the wing about the center of gravity. Thus, with AAW, the horizontal tail no longer serves to provide the pitchup moment necessary for trim. Rather, the TEO surface, deflecting negatively, does that, and the horizontal tail carries some of the lift, thereby relieving the load on the wing.

Table 5 shows the final gear ratios for the supersonic roll. In this case, the LEO surface is the independent surface to which the others are geared, and it deflects in a positive manner (nose up) to produce positive roll moment. The integrated approach favors heavier usage of all of the control surfaces relative to the LEO surface as indicated by the higher gear ratios. As a result, the deflection angle of the LEO surface necessary to trim the aircraft to the steady-state roll is much smaller for the integrated approach than it is for the sequential approach. This has a tendency to distribute the load across the wing more favorably and avoid local buildups of stress and strain that may occur in the sequential approach with its minimization of total hinge moment. Both approaches do arrive at minimal use of the trailing-edge surfaces because, at supersonic speeds, these surfaces have little effectiveness.

Finally, Fig. 8 shows the iteration history of the gear ratio design variables for the subsonic roll, and Table 6 shows the corresponding final control surface deflections. As with the subsonic pullup, both approaches arrive at significantly different solutions. Both make use of the leading-edge surfaces, even though their roll effectiveness is very low at this subsonic dynamic pressure. The reason for this significant use of the leading-edge surfaces is that they are needed to supplement the trailing-edge surfaces, which have very low effectiveness due to the thin wing (3% thickness ratio) and the very flexible structure at the final iteration. This is also observed in the iteration history, particularly for the integrated approach, as the leading-edge gear ratios increase over the course of the optimization.

The major differences between the two approaches are in their use of the trailing-edge surfaces. The sequential approach actually uses the TEI surface in a reversed fashion, even though the surface's roll effectiveness is still positive, to alleviate hinge moments. The positive deflection of the TEO surface results in negative hinge moment on itself and on the TEI surface. As a result, trim optimization, with its objective of minimizing total hinge moments, pushes the TEI surface to deflect negatively, producing positive hinge moment and counteracting the negative hinge moment contribution from the TEO surface. Hence, the hinge moment of the TEI surface is negligible for this maneuver. The integrated approach favors positive deflection of the TEI surface because it tends to relieve strain and provide increased roll moment. In fact, over the course of the optimization, the integrated approach uses it increasingly more positively, even more than the TEO surface, as indicated by its large gear ratio at the final iteration.

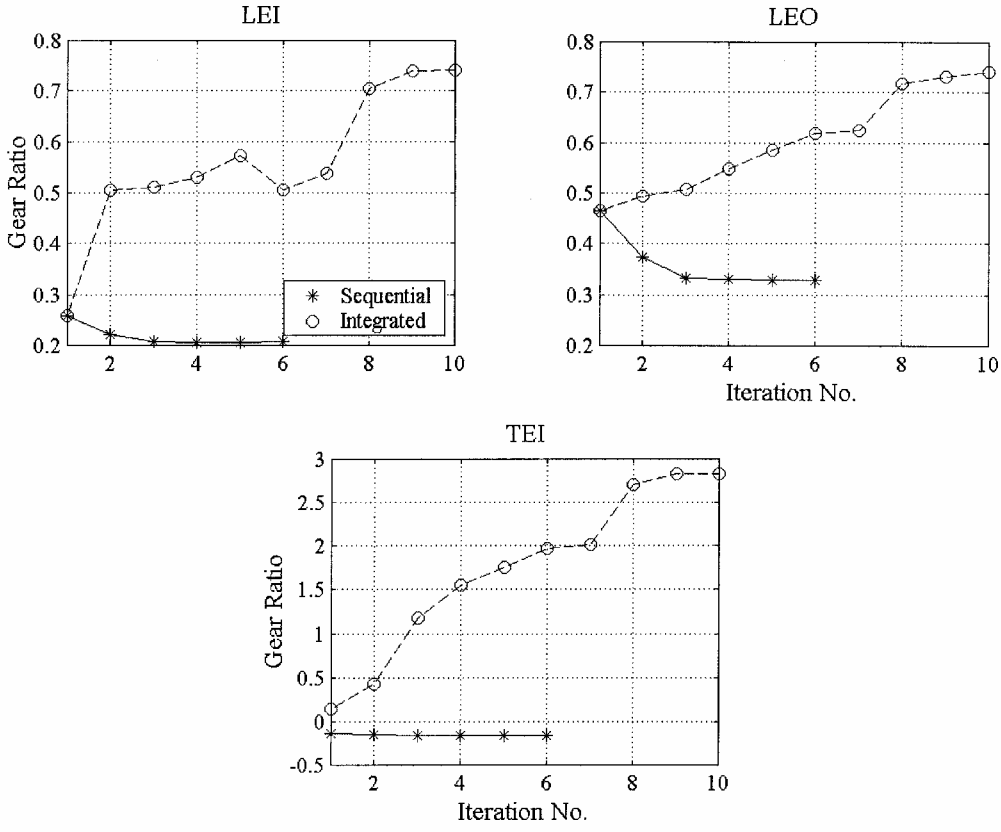

Fig. 8 Gear ratio history, subsonic roll.

The gear ratios and control surface deflection scenarios of the maneuvers presented may have been somewhat different were the internal structure and/or control surfaces designed as well. This rather simplistic design study demonstrates how the different objectives of the integrated and sequential approaches drive the design process into different control scenarios along with different optimized structural designs. A final, more practical, advantage of the integrated approach is that the concurrent optimization of the structure and gear ratios takes place in a single continuous run, in contrast to the sequential approach that requires pausing and restarting ASTROS, exchanging data, and performing trim optimization in a separate module. In addition, the integrated approach frees the user from selecting a trim optimization objective that may not contribute to a maximal reduction in weight.

Conclusions

A new integrated AAW design process, in which gear ratios and structural elements are simultaneously designed to minimize structural weight, is presented. The integrated approach differs from the sequential approach traditionally used for AAW design, in which trim optimization is performed separately from the structural optimization and is based on an independent objective function. The integrated AAW design process is implemented in the modal-based version of ASTROS by adding the gear ratios as design variables into the optimization and deriving and implementing the associated sensitivities and constraints.

Demonstration on a lightweight fighter design performing four symmetric and antisymmetric maneuvers has shown that the integrated approach results in trim scenarios that act to relieve strain in the wing's structural elements. This is opposed to the sequential approach, which results in trim scenarios that support the objectives that are defined for trim optimization, which in the case of this study are the minimization of RBM and total hinge moment for the symmetric and antisymmetric maneuvers, respectively. Consequently, optimization using the integrated design process results in a lower weight structural design. It is possible that the sequential approach may have converged to a lower weight solution than that presented if a different trim optimization objective had been used, such as one that acts toward minimizing strains. Nonetheless, the integrated approach is advantageous in that it frees the user from defining a complicated trim optimization objective and is performed in one continuous run, thereby avoiding the pause and restart required of the sequential process.

Acknowledgments

The authors extend thanks to Mordechay Karpel and Boris Moulin of Technion–Israel Institute of Technology for their technical advice and programming assistance.

References

[1]Miller, G. D., "Active Flexible Wing (AFW) Technology," U.S. Air Force Wright Aeronautical Lab., TR-87-3096, Dayton, OH, Feb. 1988.

[2]Perry, B., III, Cole, S. R., and Miller, G. D., "A Summary of an AFW Program," *Journal of Aircraft*, Vol. 32, No. 1, 1995, pp. 10–15.

[3]Pendleton, E. W., Bessette, D., Field, P. B., Miller, G. D., and Griffin, K. E., "Active Aeroelastic Wing Flight Research Program: Technical Program and Model Analytical Development," *Journal of Aircraft*, Vol. 37, No. 4, 2000, pp. 554–561.

[4]Flick, P. M., Love, M. H., and Zink, P. S., "The Impact of Active Aeroelastic Wing Technology on Conceptual Aircraft Design," *Proceedings of the RTO Applied Vehicle Technology Specialists' Meeting on Structural Aspects of Flexible Aircraft Control*, RTO MP-36, NATO Research and Technology Agency, Ottawa, Canada, Oct. 1999.

[5]Bisplinghoff, R. L., Ashley, H., and Halfman, R. L., *Aeroelasticity*, Dover, Mineola, New York, 1955, pp. 11–13.

[6]Miller, G. D., "An Active Flexible Wing Multi-Disciplinary Design Optimization Method," AIAA Paper 94-4412, Sept. 1994.

[7]Volk, J., and Ausman, J., "Integration of a Generic Flight Control System into ASTROS," AIAA Paper 96-1335, April 1996.

[8]Ausman, J., and Volk, J., "Integration of Control Surface Load Limiting into ASTROS," AIAA Paper 97-1115, April 1997.

[9]Love, M. H., Barker, D. K., Egle, D. D., Neill, D. J., and Kolonay, R. M., "Enhanced Maneuver Airloads Simulation for the Automated Structural Optimization System—ASTROS," AIAA Paper 97-1116, April 1997.

[10]Zink, P. S., Mavris, D. N., and Raveh, D. E., "Maneuver Trim Optimization Techniques for Active Aeroelastic Wings," *Journal of Aircraft*, Vol. 38, No. 6, 2001, pp. 1139–1146.

[11]Zillmer, S., "Integrated Multidisciplinary Optimization for Active Aeroelastic Wing Design," U.S. Air Force Wright Aeronautical Lab., WL-TR-97-3087, Dayton, OH, Aug. 1997.

[12]Dobbs, S. K., Schwanz, R. C., and Abdi, F., "Automated Structural Analysis Process at Rockwell," *Proceedings of the 82nd Meeting of the AGARD Structures and Materials Panel on Integrated Airframe Design Technology*, Rept. 814, AGARD, NATO Sesimbra, Portugal, 1996.

[13]Rodden, W. P., and Johnson, E. H., "MSC/NASTRAN Version 68 Aeroelastic Analysis User's Guide," Macneal–Schwendler Corp., Pasadena, CA, 1994.

[14]Neill, D. J., Johnson, E. H., and Canfield, R., "ASTROS: A Multidisciplinary Automated Design Tool," *Journal of Aircraft*, Vol. 27, No. 12, 1990, pp. 1021–1027.

[15]Zink, P. S., Mavris, D. N., Flick, P. M., and Love, M. H., "Development of Wing Structural Weight Equation for Active Aeroelastic Wing Technology," *SAE Transactions—Journal of Aerospace*, Vol. 108, No. 1, 1999, pp. 1421–1431.

[16]Dantzig, G. B., Orden, A., and Wolfe, P., "The Generalized Simplex Method for Minimizing a Linear Form Under Linear Inequality Restraints," *Pacific Journal of Mathematics*, Vol. 5, No. 1, 1955, pp. 183–195.

[17]Karpel, M., Moulin, B., and Love, M. H., "Modal-Based Structural Optimization with Static Aeroelastic and Stress Constraints," *Journal of Aircraft*, Vol. 34, No. 3, 1997, pp. 433–440.

[18]Karpel, M., "Modal-Based Enhancement of Integrated Design Optimization Schemes," *Journal of Aircraft*, Vol. 35, No. 3, 1998, pp. 437–444.

[19]Vanderplaats, G. N., "Efficient Feasible Directions Algorithm for Design Synthesis," *AIAA Journal*, Vol. 22, No. 11, 1984, pp. 1633–1640.

[20]Karpel, M., "Modal-Based Structural Optimization Using ASTROS—Theoretical Manual," Technion–Israel Inst. of Technology, TAE 795, Haifa, Israel, Sept. 1997.

[21]Johnson, E. H., and Venkayya, V. B., "Automated Structural Optimization System (ASTROS), Vol. 1—Theoretical Manual," U.S. Air Force Wright Aeronautical Lab., AFWAL-TR-88-3028, Dayton, OH, Dec. 1988.

[22]Rodden, W. P., and Love, J. R., "Equations of Motion of Quasisteady Flight Vehicle Utilizing Restrained Static Aeroelastic Characteristics," *Journal of Aircraft*, Vol. 22, No. 9, 1995, pp. 802–809.

[23]"Optimization Toolbox for Use with MATLAB—User's Guide, Version 2," The MathWorks, Inc., Natick, MA, 1999.

[24]Chvátal, V., *Linear Programming*, W. H. Freeman, New York, 1983, p. 222.

[25]Zink, P. S., Mavris, D. N., Love, M. H., and Karpel, M., "Robust Design for Aeroelastically Tailored/Active Aeroelastic Wing," AIAA Paper 98-4781, Sept. 1998.

[26]Carmichael, R. L., Castellano, C. R., and Chen, C. F., "The Use of Finite Element Methods for Predicting the Aerodynamics of Wing–Body Combinations," NASA SP-228, Oct. 1969.

[27]Barker, D. K., and Love, M. H., "An ASTROS Application with Path Dependent Results," AIAA Paper 96-4139, Sept. 1996.

[28]Zink, P. S., "A Methodology for Robust Structural Design with Application to Active Aeroelastic Wings," Ph.D. Dissertation, Georgia Inst. of Technology, School of Aerospace Engineering, Atlanta, GA, June 2001.